https://doi.org/10.5194/essd-2026-502
Preprint. Discussion started: 25 November 2026
© Author(s) 2026. CC BY 4.0 License.



Open Access Earth System Science Data Discussions

High-resolution BIOCLIM and ENVIREM grids for Europe in the last 21,000 years: downscaled CCSM3 simulations compared to pollen-based reconstructions

Jan Divíšek[1,2], Michal Hájek[1], Michal Horsák[1], Petra Hájková[1,3]

[1]Department of Botany and Zoology, Masaryk University, Brno, 602 00, Czech Republic
[2]Department of Geography, Masaryk University, Brno, 602 00, Czech Republic
[3]Department of Paleoecology, Institute of Botany, The Czech Academy of Sciences, Brno, 602 00, Czech Republic

Correspondence to: Jan Divíšek (divisekjan@sci.muni.cz)

Abstract. High-resolution paleoclimatic data are essential for understanding how past climate changes have shaped modern biodiversity and for developing robust models to predict future biotic responses. Here, we introduce a comprehensive dataset of paleoclimate grids for Europe covering the last 21,000 years, from the Last Glacial Maximum to the present. This dataset goes beyond the commonly used set of 19 bioclimatic (BIOCLIM) variables by incorporating an additional 16 environmental (ENVIREM) variables, which have been identified as biologically relevant factors influencing the ecological or physiological processes that determine species distributions. The complete set of 35 variables is provided at a high spatial resolution of 30 arc-seconds in transient 100-year temporal steps. These variables were calculated from monthly temperature and precipitation simulations of the Community Climate System Model version 3, which were statistically downscaled and debiased using a change-factor approach based on high-resolution baseline climate data. Technical validation against alternative paleoclimate databases confirms high spatial and temporal congruence across the dataset, with minor discrepancies limited to variables dependent on the identification of the wettest quarter of the year. Additionally, we evaluated temperature and precipitation simulations against pollen-based reconstructions from the Temperature 12k database across 137 sites in Europe. The comparison shows that model-proxy agreement is highly variable across both time and space and depends on whether annual means or seasonal variables are considered. This open-access dataset, freely available at https://doi.org/10.5281/zenodo.5119958 (Divíšek, 2021), enables the integration of transient climate dynamics into paleoecological and biogeographical models, enhancing their capacity to track biotic responses to past climate changes.

1 Introduction

Climate is considered a primary driver of species distributions on Earth, and it is widely acknowledged that climatic changes during the Quaternary substantially shaped present-day biota (Fordham et al., 2018; Svenning et al., 2015). Major biotic changes occurred, particularly at interglacial–glacial transitions, where near-complete replacement of species and communities responded to abrupt climate shifts. In this regard, the Pleistocene–Holocene transition appears to be of prime importance for

https://doi.org/10.5194/essd-2026-502
Preprint. Discussion started: 25 November 2026
© Author(s) 2026. CC BY 4.0 License.

Open Access Earth System Science Data Discussions

the development of modern biotic communities (Blois et al., 2013b; Cooper et al., 2015; Fordham et al., 2020; Hewitt, 2000; Williams et al., 2004). However, substantial changes in species distributions continued mainly during the first half of the Holocene due to the spread of temperate species from glacial refugia (Bennett et al., 1991; Horsák et al., 2020; Schmitt and Varga, 2012) as well as extinctions and altitudinal shifts of cold-adapted species, still surviving in lowlands during the Early Holocene (Juřičková et al., 2014b; Ložek, 1964). High-resolution paleoclimatic data are thus essential for investigating and understanding these processes and developing effective models to predict changes in biotic communities under future climate change.

Paleoclimatic data usually come from downscaled simulations with General Circulation Models (GCMs), which are often run for a limited number of climatically distinct time windows (climate snapshots), including the middle Pliocene, Last Interglacial, Last Glacial Maximum (LGM) or mid-Holocene. While ecological impacts of late Quaternary climate dynamics are frequently assessed using discrete time slices separated by 1,000-year intervals (Blois et al., 2013a; Veloz et al., 2012), such coarse temporal sampling often fails to capture species responses to shorter, centennial-scale climatic oscillations that nonetheless carry substantial biological consequences (Fordham et al., 2017, 2018). These include not only rapid climate shifts during the Pleistocene–Holocene transition such as Heinrich Event 1, Bølling–Allerød or Younger Dryas but also less pronounced fluctuations during the Holocene (Mayewski et al., 2004), such as the "8 ka" (Alley and Ágústsdóttir, 2005) or the "4.2 ka" (Magny et al., 2009) events. While the scientific community has made significant strides in data accessibility, a trade-off between spatial and temporal resolution has persisted. For instance, Lorenz et al. (2016) provided high-temporal-resolution simulations for North America based on the Community Climate System Model version 3 (CCSM3; Collins et al., 2006), yet the spatial resolution of 0.5° remains a limiting factor for regional paleoecological studies or high-accuracy Species Distribution Models (SDM). Similarly, the PaleoView software (Fordham et al., 2017) have made CCSM3 simulations at high temporal resolutions starting from 10 years easily available, but its coarse spatial resolution of 2.5° is insufficient for capturing the topographically driven climatic variation. To address spatial limitations, the PaleoClim database (Brown et al., 2018) downscaled CCSM3 simulations to a relatively high spatial resolution of 2.5 arc-minutes (~5 km). However, PaleoClim offers only a limited number of time slices – six windows 1,200–4,126 years wide for the last 17,000 years – which can mask the continuous climatic dynamics essential for tracking species migrations from glacial refugia. Recently, the CHELSA-TraCE21k dataset (Karger et al., 2023) established a new global benchmark by providing transient data at a 1 km spatial resolution in 100-year windows covering the period from 21,000 BP to the present.

Climate variables used to track biotic responses to past climate change should ideally represent biologically relevant factors linked to ecological or physiological processes that determine species niches. The 19 BIOCLIM variables, originally defined within BIOCLIM software (Nix, 1986), part of the ANUCLIM package (Xu and Hutchinson, 2011), are perhaps the most widely used environmental data layers for this purpose. These variables are available in the WorldClim (Hijmans et al., 2005) and CHELSA (Karger et al., 2017) databases for the present period as well as in CHELSA-TraCE21k-centennial-bioclim dataset (Karger et al., 2023) as transient high-resolution simulations for the last 21,000 years. This set of BIOCLIM variables has been extended by Title and Bemmels (2018) by providing 16 environmental rasters for ecological modeling (ENVIREM)

https://doi.org/10.5194/essd-2026-502
Preprint. Discussion started: 25 November 2026
© Author(s) 2026. CC BY 4.0 License.

Open Access Earth System Science Data Discussions

accompanying the WorldClim dataset for present, mid Holocene and LGM periods. Also Brun et al. (2022) extended BIOCLIM variables by calculating additional set of variables, but only for the present period. These datasets highlight the importance of seasonal variables, such as growing-season temperature or summer/winter temperatures, over annual means, which often fail to capture key physiological processes that directly limit species growth and persistence. For example, it has been suggested that the apparent divergence between proxy-based reconstructions of Holocene temperature and model simulations may reflect the response of biotic proxies, such as pollen, to seasonal – primarily summer – temperatures rather than annual means (Bova et al., 2021; Liu et al., 2014b). The availability of a wide range of paleoclimatic variables at high spatial and temporal resolution is therefore essential for capturing important limiting factors that may constrain the distributions of individual species and entire communities.

Here, we introduce a comprehensive set of paleoclimate grids for Europe, including 19 BIOCLIM and 16 ENVIREM variables at a high spatial resolution of 30 arc-seconds (~1 km) and a temporal resolution of 100 years. This dataset covers the entire European continent and adjacent regions within 32.5°W–70°E and 32.5°N–82.5°N and spans the period from 21,000 to present. BIOCLIM and ENVIREM variables were calculated using downscaled and debiased monthly temperature and precipitation simulations from the Community Climate System Model version 3 (CCSM3; Collins et al., 2006) and validated against relevant published datasets. Simulations of mean annual, January, and July temperatures, as well as annual precipitation amounts, are also compared with pollen-inferred reconstructions from the Temperature 12k database (Kaufman et al., 2020a), identifying specific regions and periods where model outputs align with or deviate from reconstructed temperature and precipitation. By providing this comprehensive high-resolution dataset, we aim to facilitate the application of climate-based ecological models for any period between the LGM and the present, and to support the investigation of dynamic spatio-temporal gradients that have shaped European biodiversity.

2 Methods

2.1 Paleoclimate simulations

Paleoclimate model outputs utilized in this study originate from the TraCE-21ka transient simulation (Liu et al., 2014a; Otto-Bliesner et al., 2014), conducted with the Community Climate System Model version 3 (CCSM3; Collins et al., 2006; Otto-Bliesner et al., 2006; Yeager et al., 2006), which couples atmosphere, ocean, sea-ice, and land-surface components at a global scale. We extracted these gridded outputs via PaleoView version 1.5.1 (Fordham et al., 2017). The TraCE-21ka experiment was driven by variations in orbital insolation, shifting atmospheric concentrations of major greenhouse gases (carbon dioxide, methane, and nitrous oxide), and dynamic changes in continental ice-sheet extent along with freshwater meltwater fluxes into the oceans, whereas volcanic activity and variations in total solar irradiance were not incorporated (Fordham et al., 2017). The data we accessed include minimum, mean, and maximum monthly temperatures, as well as monthly precipitation amounts for centennial (100-year) time windows that consecutively cover the last 21,000 years. These windows are centered on calendar centuries, with the most recent centennial window, 100–0 BP, corresponding to 1850–1950 CE and centered on 50 BP, i.e.

https://doi.org/10.5194/essd-2026-502
Preprint. Discussion started: 25 November 2026
© Author(s) 2026. CC BY 4.0 License.

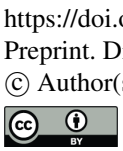

Open Access Earth System Science Data Discussions

1900 CE. The data are provided at a spatial resolution of 2.5° × 2.5° and were generated for the area from 32.5°W to 70°E and from 32.5°N to 82.5°N (Fig. 1). In total, we downscaled 10,080 gridded paleoclimatic simulations.

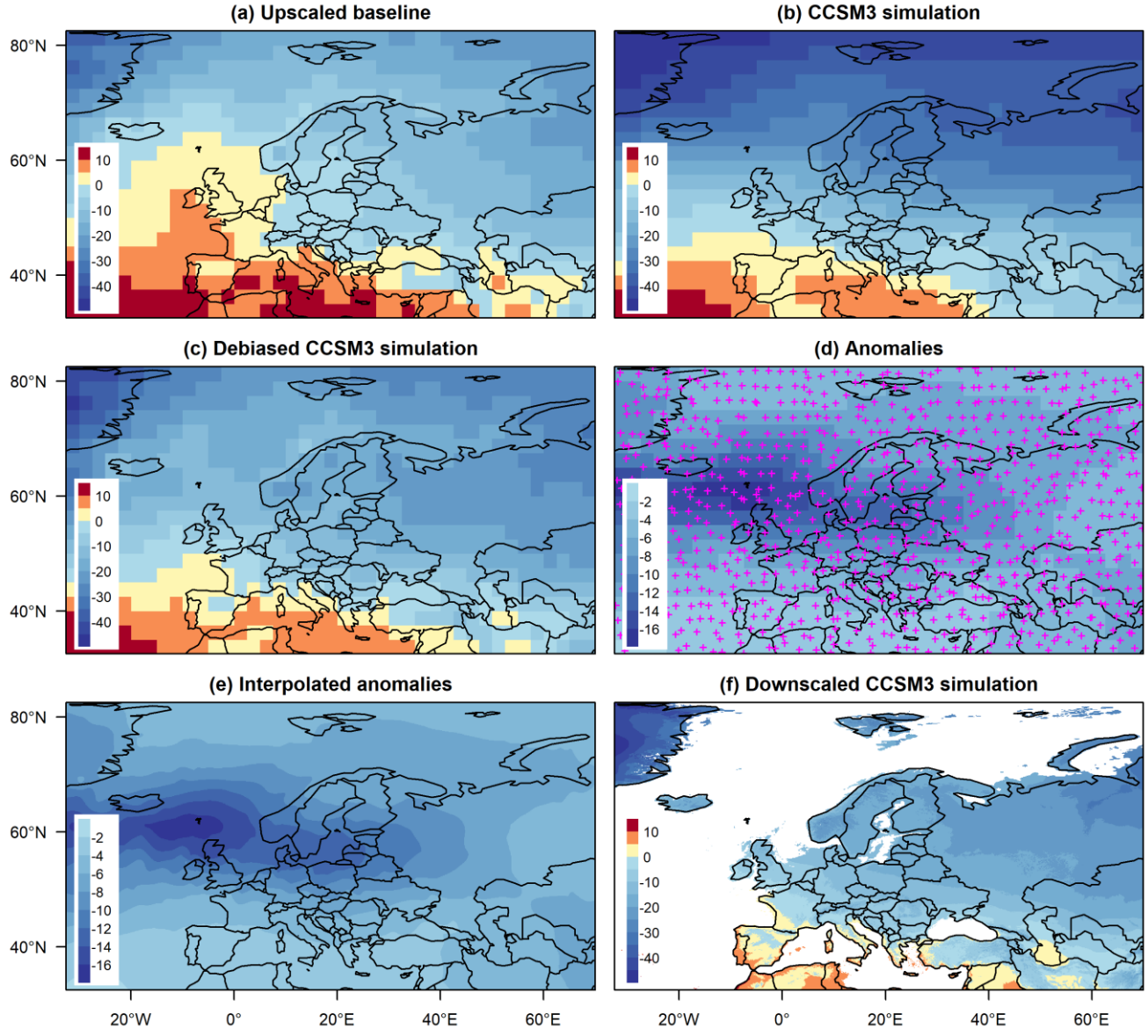

Figure 1: Illustration of the downscaling process with mean January temperature (°C). (a) Baseline data from the CHELSA database (1940–1989 CE) upscaled to 2.5° resolution. (b) CCSM3 simulation for the onset of the Holocene at 2.5° resolution. (c) Debiased CCSM3 simulation. (d) Anomalies at the onset of the Holocene with interpolation points overlaid. (e) Anomalies at a resolution of 30 arc-seconds interpolated using Multilevel B-spline interpolation. (f) Downscaled mean January temperature grid at 30 arc-second resolution. The grid is clipped to the land extent estimated from sea-level changes published by Lambeck et al. (2014). The maps were created by the authors using data from PaleoView (Fordham et al., 2017) and CHELSA (Karger et al., 2017) with state borders from the rworldmap R package (South, 2011).

https://doi.org/10.5194/essd-2026-502
Preprint. Discussion started: 25 November 2026
© Author(s) 2026. CC BY 4.0 License.



2.2 Baseline climatic data

As baseline data representing current climatic conditions, we used monthly minimum, mean, and maximum temperature and monthly precipitation grids at a resolution of 30 arc-seconds (~1 km) from the CHELSA database (version 1.2; Karger et al., 2017). We used the CHELSA Timeseries and CHELSAcruts datasets to calculate monthly 50-year averages for the period from 1940 to 1989 CE.

Covering the period 1979–2013 CE, the CHELSA Timeseries dataset provides monthly temperature and precipitation grids derived by downscaling the ERA-Interim reanalysis (Karger et al., 2017). Specifically, air temperatures were estimated via statistical downscaling, whereas the downscaling algorithm for precipitation integrated key topographic and boundary-layer controls – namely wind fields, valley exposure, and planetary boundary layer height – followed by an empirical bias-correction step (Karger et al., 2017). CHELSAcruts is a downscaled CRU TS 4.01 dataset of monthly maximum and minimum temperatures, and monthly precipitation sums for each year from 1901 to 2016 CE. It does not account for changing wind patterns or temperature lapse rates, but instead assumes they are constant over time and similar to the long-term averages. Because this dataset does not contain monthly mean temperatures, we estimated them as the arithmetic mean of monthly minimum and maximum temperatures.

2.3 Statistical downscaling

To downscale the CCSM3 simulations described above, we used the change-factor approach (Ramirez Villejas and Jarvis, 2010). This method relies on quantification of differences (anomalies or deltas) between the coarse-resolution simulation provided by the GCM and the baseline climate data at the same resolution. Differences between the baseline and the GCM simulation for current period are used to correct for GCM bias, while the differences between the debiased GCM simulation for historical period and the baseline are used for calculating high-resolution paleoclimatic grids. In this procedure, coarse-scale anomalies are interpolated between centers of GCM grid cells and then added (or multiplied, in the case of relative differences) to baseline climatic data at high resolution. The method thus assumes that changes in climate are relevant only at coarse scales and that the fine-scale spatial pattern of baseline data remains consistent over time (Karger et al., 2017; Ramirez Villejas and Jarvis, 2010).

First, to account for bias in the CCSM3 simulation (Cannon et al., 2015; Maraun, 2013), we upscaled high-resolution baseline CHELSA grids to the resolution of 2.5° (Fig. 1a). Temperature grids were upscaled using arithmetic averaging while precipitation grids using the calculation of median value. Then we calculated absolute (for temperatures) or relative (for precipitation) differences between upscaled CHELSA data and CCSM3 simulation for the period 1940–1989 CE. This so-called bias layer was then added (in the case of temperatures) or multiplied (in the case of precipitation) to CCMS3 grids (Fig. 1b), resulting in debiased CCSM3 simulation (Fig. 1c). Subsequently, we calculated the differences between the debiased CCSM3 simulation for each centennial time window up to 21,000 BP and the upscaled CHELSA baseline, resulting in an anomaly layer at a resolution of 2.5° for each period (Fig. 1d). Anomalies are usually interpolated among cell centroids and

https://doi.org/10.5194/essd-2026-502
Preprint. Discussion started: 25 November 2026
© Author(s) 2026. CC BY 4.0 License.



then added (or multiplied) to a high-resolution baseline climate grid (Ramirez Villejas and Jarvis, 2010). Instead of using centroids, we used an approach similar to that of Moreno and Hasenauer (2016) and identified the point inside each 2.5° cell that meets the following criteria: 1) The value of high-resolution (30 arc-seconds) baseline CHELSA grid at this point matches the value of the respective cell of upscaled CHELSA grid at a 2.5° resolution. 2) If two or more points fulfilled the first criterion, the point closest to the centroid of the 2.5° cell was selected. Anomalies were assigned to these points and interpolated using the Multilevel B-spline algorithm for scattered data as proposed by Lee et al. (1997). The resulting grids at a resolution of 30 arc-seconds were then added (for temperatures) or multiplied (for precipitation) to the respective CHELSA grid with the same resolution. Using this procedure, we prepared debiased high-resolution grids of monthly minimum, mean, and maximum temperatures, and monthly precipitation simulations for Europe and 210 centennial time windows consecutively covering the last 21,000 years. These grids were clipped to land extent, which was estimated for each time window based on sea level changes published by Lambeck et al. (2014). The statistical downscaling was performed in SAGA version 6.3.0 (Conrad et al., 2015) and R software version 3.6.0 (R Core Team, 2022) using RSAGA (Brenning et al., 2018) and raster (Hijmans, 2019) packages.

Table 1: List of BIOCLIM and ENVIREM variables calculated from downscaled simulations of monthly temperatures and precipitation amounts provided by the CCSM3. Values of some variables were multiplied by a scaling factor to reduce data size while maintaining sufficient precision.

Abbreviation	Description	Units	Scaling factor
bio1	Annual mean temperature	°C	10
bio2	Mean diurnal range (mean of monthly (max temp - min temp))	°C	10
bio3	Isothermality (BIO2/BIO7)	°C × 100	10
bio4	Temperature seasonality (standard deviation)	°C × 100	10
bio5	Maximum temperature of the warmest month	°C	10
bio6	Minimum temperature of the coldest month	°C	10
bio7	Temperature annual range (BIO5 - BIO6)	°C	10
bio8	Mean temperature of the wettest quarter	°C	10
bio9	Mean temperature of the driest quarter	°C	10
bio10	Mean temperature of the warmest quarter	°C	10
bio11	Mean temperature of the coldest quarter	°C	10
bio12	Annual precipitation	mm / year	
bio13	Precipitation of the wettest month	mm / month	
bio14	Precipitation of the driest month	mm / month	
bio15	Precipitation seasonality (coefficient of variation)	-	
bio16	Precipitation of the wettest quarter	mm / quarter	
bio17	Precipitation of the driest quarter	mm / quarter	
bio18	Precipitation of the warmest quarter	mm / quarter	
bio19	Precipitation of the coldest quarter	mm / quarter	

https://doi.org/10.5194/essd-2026-502
Preprint. Discussion started: 25 November 2026
© Author(s) 2026. CC BY 4.0 License.



Open Access Earth System Science Data Discussions

annualPET	Annual potential evapotranspiration: a measure of the ability of the atmosphere to remove water through evapotranspiration processes, given unlimited moisture	mm / year	
aridityIndexThornthwaite	Thornthwaite aridity index: Index of the degree of water deficit below water need	-	10
climaticMoistureIndex	A metric of relative wetness and aridity	-	1000
continentality	Average temperature of the warmest month - average temperature of the coldest month	°C	10
embergerQ	Emberger's pluviothermic quotient: a metric that was designed to differentiate among Mediterranean type climates	-	
growingDegDays0	Sum of mean monthly temperature for months with mean temperature greater than 0°C multiplied by the number of days	°C	
growingDegDays5	Sum of mean monthly temperature for months with mean temperature greater than 5°C multiplied by the number of days	°C	
maxTempColdest	Maximum temperature of the coldest month	°C	10
minTempWarmest	Minimum temperature of the warmest month	°C	10
monthCountByTemp10	Count of the number of months with mean temperature greater than 10°C	months	
PETColdestQuarter	Mean monthly PET of the coldest quarter	mm / quarter	
PETDriestQuarter	Mean monthly PET of the driest quarter	mm / quarter	
PETseasonality	Monthly variability in potential evapotranspiration	mm / quarter × 100	
PETWarmestQuarter	Mean monthly PET of the warmest quarter	mm / quarter	
PETWettestQuarter	Mean monthly PET of the wettest quarter	mm / quarter	
thermicityIndex	Compensated thermicity index: sum of mean annual temperature, minimum temperature of the coldest month, maximum temperature of the coldest month, × 10, with compensations for better comparability across the globe	°C × 10	

2.4 BIOCLIM and ENVIREM variables

For each centennial window up to 21,000 BP, downscaled and debiased monthly temperature and precipitation simulations were used to calculate a set of 35 biologically meaningful BIOCLIM (Nix, 1986) and ENVIREM (Title & Bemmels, 2018) variables suitable for species distribution modelling and other ecological applications (Table 1). Variable definitions followed those in the WorldClim database (Hijmans et al., 2005) and the ANUCLIM software package (Xu and Hutchinson, 2011) for BIOCLIM variables, and those published by Title and Bemmels (2018) for ENVIREM variables. Temperature seasonality (bio4) follows the WorldClim definition and was calculated as the standard deviation of monthly mean temperatures, rather than the coefficient of variation used in ANUCLIM. Because the calculation of ENVIREM variables requires monthly extraterrestrial solar radiation, these data were obtained from the palinsol R package (Crucifix, 2016). Collectively, these variables capture long-term annual means (such as mean annual temperature, annual precipitation, and annual PET), intra-annual variability (e.g., temperature and precipitation seasonality), and climatic extremes or physiological limits (such as the temperatures of the warmest and coldest months). Rather than corresponding to fixed calendar seasons, quarterly metrics are computed over rolling windows of any three consecutive months. All variables were calculated in SAGA version 6.3.0 (Conrad

https://doi.org/10.5194/essd-2026-502
Preprint. Discussion started: 25 November 2026
© Author(s) 2026. CC BY 4.0 License.

et al., 2015) using the equations described here: https://zenodo.org/records/5119958/files/Technical_specification.pdf?download=1.

2.5 Technical validation against published paleoclimate grids

We validated BIOCLIM variables against those from the CHELSA-TraCE21k-centennial-bioclim dataset (Karger et al., 2023; https://www.chelsa-climate.org/datasets/chelsa-trace21k-centennial-bioclim) and the PaleoClim database (Brown et al., 2018; http://www.paleoclim.org/), both based on simulations of the CCSM3, to evaluate discrepancies and potential biases introduced by differing downscaling procedures and baseline climatologies. CHELSA-TraCE21k-centennial-bioclim is a global dataset of BIOCLIM variables provided in centennial time windows for the last 21,000 years at a spatial resolution of 30 arc-seconds (~1 km). This dataset was produced by downscaling transient TraCE-21k outputs using the CHELSA v1.2 methodology. The workflow explicitly reconstructs time-varying paleo-orography by coupling the ICE-6G_C glacial isostatic adjustment model with global sea-level records and GMTED2010 elevation data, thereby capturing shifting ice sheets and shorelines across individual time windows. Systematic model bias in temperature and precipitation simulations was mitigated using a change-factor adjustment calibrated against CHELSA v1.2 reference grids for the period 1980–1990 CE. BIOCLIM variables were subsequently derived from the downscaled and debiased monthly temperature and precipitation grids. Because Karger et al. (2023) delineate centennial windows along calendar centuries, resulting in a 50-year offset relative to our temporal windows, we computed the mean of each pair of consecutive layers in CHELSA-TraCE21k-centennial-bioclim to ensure direct temporal correspondence.

The PaleoClim database provides BIOCLIM variables for six periods of varying length in the late Pleistocene and Holocene: Heinrich Stadial 1 (17,000–14,700 BP), Bølling-Allerød (14,700–12,900 BP), Younger Dryas Stadial (12,900–11,700 BP), early-Holocene, Greenlandian (11,700–8,326 BP), mid-Holocene, Northgrippian (8,326–4,200 BP), and late-Holocene, Meghalayan (4,200–300 BP). PaleoClim uses a change-factor approach to downscale CCSM3 simulations. HadCM3 control simulations were used to express climate changes from pre-industrial conditions. These anomalies were then added to CHELSA v1.2 data to produce downscaled temperature and precipitation grids, and then used to calculate BIOCLIM variables, which are provided at a spatial resolution of 2.5 arc-minutes (~5 km). To match the coarser temporal resolution of the PaleoClim data, we averaged each BIOCLIM variable from our dataset across all centennial time windows falling within each respective PaleoClim period.

ENVIREM variables could not be compared with any other source of data using transient simulations of the CCSM3. Therefore, we compared them with the ENVIREM variables for the LGM and mid-Holocene snapshots derived from three different GCMs, namely CCSM4, MIROC-ESM and MPI-ESM-P, available in the ENVIREM database (Title and Bemmels, 2018; https://envirem.github.io/). These data are provided at a spatial resolution of 2.5 arc-minutes (~5 km).

For all comparisons, we used variable values at 10,000 points randomly distributed across Europe and the following metrics: First, Willmott's refined index of agreement (d_r; Willmott et al., 2012) representing the degree of spatial congruence between

https://doi.org/10.5194/essd-2026-502
Preprint. Discussion started: 25 November 2026
© Author(s) 2026. CC BY 4.0 License.



each pair of corresponding variables in each period considered. It varies between −1 and 1, with 1 indicating a perfect agreement. The index is defined as:

$$d_r = \begin{cases} 1-\frac{\sum_{i=1}^{n}|S_i-R_i|}{c\sum_{i=1}^{n}|R_i-\bar{R}|}, \text{when} \\ \sum_{i=1}^{n}|S_i-R_i| \le c\sum_{i=1}^{n}|R_i-\bar{R}| \\ \frac{c\sum_{i=1}^{n}|R_i-\bar{R}|}{\sum_{i=1}^{n}|S_i-R_i|}-1, \text{when} \\ \sum_{i=1}^{n}|S_i-R_i| > c\sum_{i=1}^{n}|R_i-\bar{R}| \end{cases}, \quad (1)$$

where S_i is the value of the BIOCLIM or ENVIREM variable we calculated based on downscaled CCSM3 simulations for location i, R_i is the value of the same variable in the reference dataset (i.e. CHELSA-TraCE21k-centennial-bioclim, PaleoClim or ENVIREM) and c = 2. Second, we used the normalized mean error (ME) to show the direction (positive or negative) of the mean difference between variable values. It was calculated as:

$$\text{Normalized ME} = \frac{\frac{1}{n}\sum_{i=1}^{n}|S_i-R_i|}{\sigma_R}, \quad (2)$$

where σ_R is the standard deviation of the reference variable. Both indices were calculated using the hydroGOF R package (Zambrano-Bigiarini, 2026).

2.6 Comparison with proxy-based reconstructions

High-resolution CCSM3 simulations produced by the downscaling procedure described above were compared with pollen-based reconstructions from the Temperature 12k database (Kaufman et al., 2020a; https://lipdverse.org/project/temp12k/) to evaluate their congruence across time and space. Most pollen-based paleotemperature time series in the database were compiled by Marsicek et al. (2018). We selected variables designated as “temperature”, “temperatureComposite” and “precipitation” with seasonality specified as “annual”, “coldest month” or “1” and “warmest month” or “7” representing reconstructions of mean annual temperature, mean temperature of the coldest month (January), mean temperature of the warmest month (July), and annual precipitation, expressed in °C and mm year−1. These variables were extracted for 137 sites across Europe, each representing a peat or lake-sediment archive with pollen-inferred time series of varying length from 4,291 to 12,655 years.

To match the centennial (100-year) resolution of the CCSM3 simulations, each pollen-based reconstruction was linearly interpolated between points with calibrated ages. However, the number of sites with available reconstructions varied across individual centennial windows, reaching a maximum during the late and mid-Holocene (136 sites) but being considerably lower in the early Holocene (Fig. 2). Therefore, comparisons were performed only up to 11,000 years BP.

Simulated and reconstructed temperature and precipitation trends over the past 11,000 years were compared by plotting mean deviations from the most recent period, i.e., 100–0 BP, to account for potential differences resulting from the use of different baselines. Absolute deviations (in °C) at each site were calculated for temperature, while relative deviations (percent change) were calculated for precipitation. For 71 sites, temperature and precipitation reconstructions did not reach the 100–0 BP period. For these sites, we estimated 100–0 BP values using the Random Forest algorithm, a highly flexible machine-learning

https://doi.org/10.5194/essd-2026-502
Preprint. Discussion started: 25 November 2026
© Author(s) 2026. CC BY 4.0 License.



technique for gap-filling meteorological data that can capture complex non-linear interactions (Boomgard-Zagrodnik and Brown, 2022; Lalic et al., 2024). We used the missForest implementation of this algorithm (Stekhoven and Bühlmann, 2012) and predicted missing values based on relationships with time series at other sites, as well as the geographical coordinates and elevation of each site. To examine regional differences in agreement between simulated and reconstructed temperature and precipitation, we used Pearson correlation and mapped the correlation coefficients across all 137 sites in Europe. For each centennial window, we then correlated spatial patterns in simulated and reconstructed temperature and precipitation values. The resulting correlation coefficients were plotted to show how the spatial patterns agreed over the last 11,000 years.

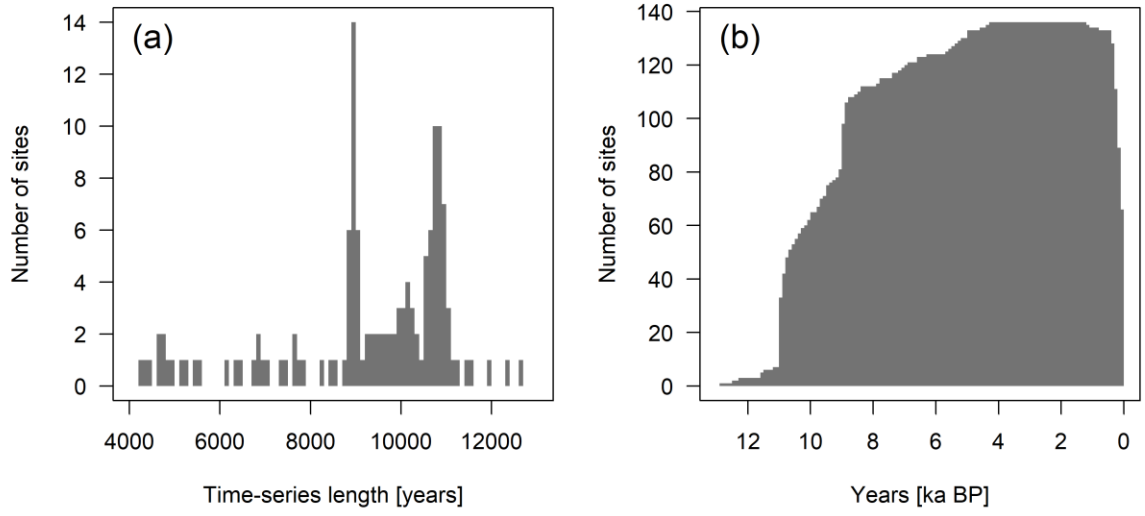

Figure 2: Frequency distribution of sites with pollen-based reconstructions of temperature and precipitation for Europe in the Temperature 12k database. (a) Distribution of time-series lengths in the dataset. (b) Number of sites within each centennial time window.

3 Results

We prepared a comprehensive dataset of high-resolution grids which contains 19 BIOCLIM and 16 ENVIREM variables (Table 1) for 210 centennial time windows covering the last 21,000 years (Fig. 3). These grids are provided at a spatial resolution of 30 arc-seconds for the area from 32.5°W to 70°E and from 32.5°N to 82.5°N. Given their high temporal resolution, these grids capture major climatic events at the Pleistocene-Holocene transition as well as finer centennial climatic fluctuations throughout the entire period and are suitable for species distribution modelling and palaeoecological research at the landscape scale.

https://doi.org/10.5194/essd-2026-502
Preprint. Discussion started: 25 November 2026
© Author(s) 2026. CC BY 4.0 License.

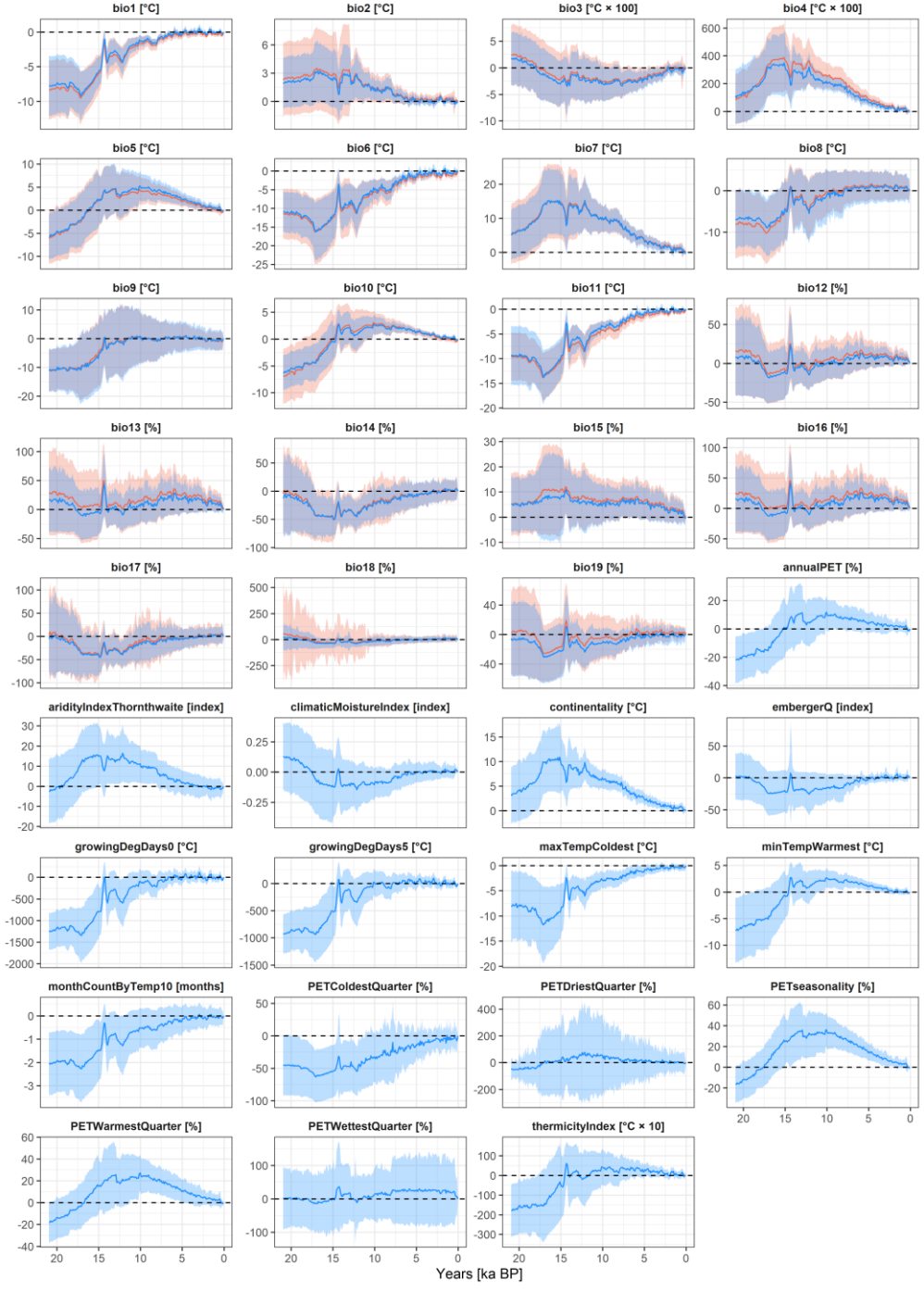

Figure 3: Late Pleistocene and Holocene changes in BIOCLIM and ENVIREM variables for Europe presented as deviations from 100–0 BP (1850–1950 CE). Blue and red curves show the mean values for downscaled CCSM3 simulations presented here and those in the CHELSA-TraCE21k-centennial-bioclim dataset, respectively. These were calculated from 10,000 points randomly distributed across Europe. Shading represents 1σ on each side of the mean. For precipitation and PET variables, deviations are expressed as percent change relative to 100–0 BP.

https://doi.org/10.5194/essd-2026-502
Preprint. Discussion started: 25 November 2026
© Author(s) 2026. CC BY 4.0 License.



Open Access Earth System Science Data Discussions

Technical validation against CHELSA-TraCE21k-centennial-bioclim showed high agreement between the datasets (Fig. 4 and 5). Across all 210 time windows, the mean Willmott's refined index of agreement for all but one BIOCLIM variable exceeded 0.8. Only the mean temperature of the wettest quarter (bio8) showed weaker agreement, with dr = 0.77 ± 0.04. Most variables presented here showed slightly lower values in the same time windows compared to those in CHELSA-TraCE21k-centennial-bioclim, but these differences were negligible (mean normalized ME was −0.13–0.08) and can likely be attributed to the use of different baseline data and downscaling algorithm. A similar result was found for BIOCLIM variables from the PaleoClim database, although it contains data for much wider time windows and coarser spatial resolution of 2.5 arc-minutes (Fig. 4). Mean Willmott's index for most variables was higher than 0.8, and mean normalized ME ranged between −0.25 and 0.3, indicating small differences between the values of most variables.

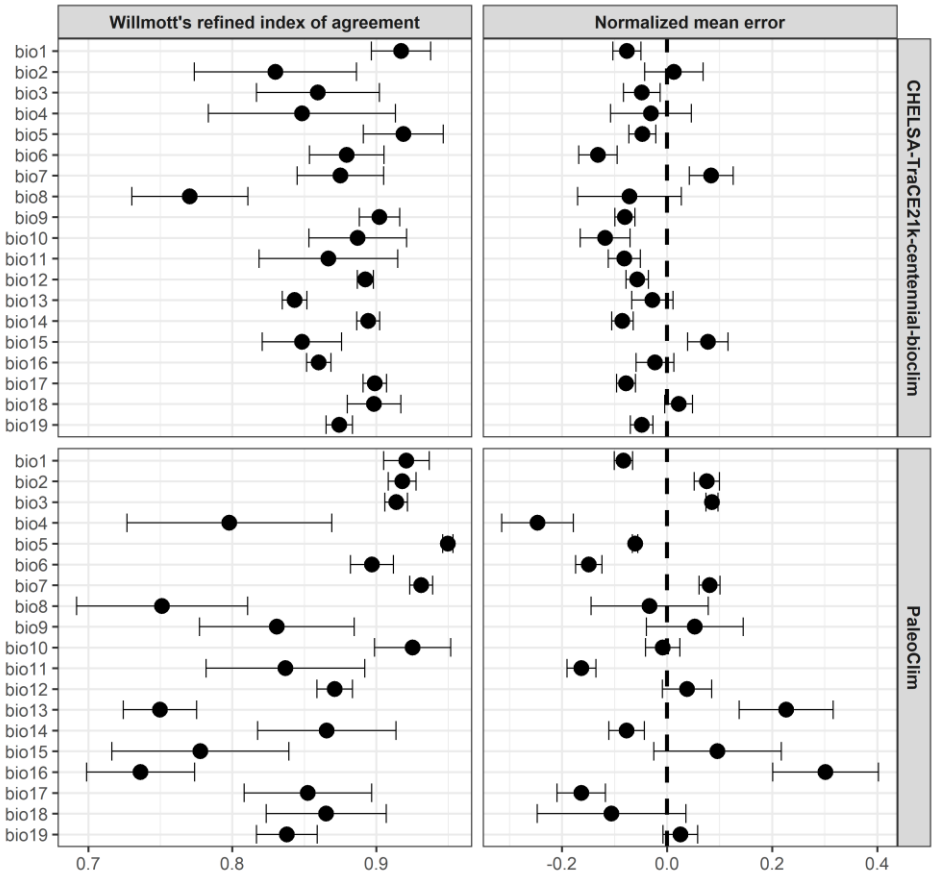

Figure 4: Technical validation of the BIOCLIM variables derived from the downscaled CCSM3 simulations against those in the CHELSA-TraCE21k-centennial-bioclim and PaleoClim databases. Willmott's refined index of agreement (d_r) shows the mean agreement of corresponding variables across all 210 centennial windows. Error bars represent 1σ on each side of the mean. Normalized ME shows the mean difference between variable values and its direction across all time windows. A negative value means that the BIOCLIM variable presented here has, on average, lower values than the same variable from the CHELSA-TraCE21k-centennial-bioclim or PaleoClim database, and vice versa. Error bars represent 1σ. Both indices were calculated based on 10,000 points randomly distributed across Europe.

https://doi.org/10.5194/essd-2026-502
Preprint. Discussion started: 25 November 2026
© Author(s) 2026. CC BY 4.0 License.



Open Access Earth System Science Data Discussions

ENVIREM variables were compared to those in the ENVIREM database for the LGM and mid-Holocene periods (Fig. 5). Although the compared variables were derived from different GCMs, Willmott's index of agreement exceeded 0.8 for most pairs. However, for PETWettestQuarter and embergerQ, the agreement dropped below 0.6, especially in comparisons with MIROC-ESM and MPI-ESM-P simulations for the LGM, indicating discrepancies in the spatial distributions of variable values. Normalized ME also showed higher variability, ranging from −0.4 to 0.6 for the LGM and from −0.31 to 0.23 for the mid-Holocene.

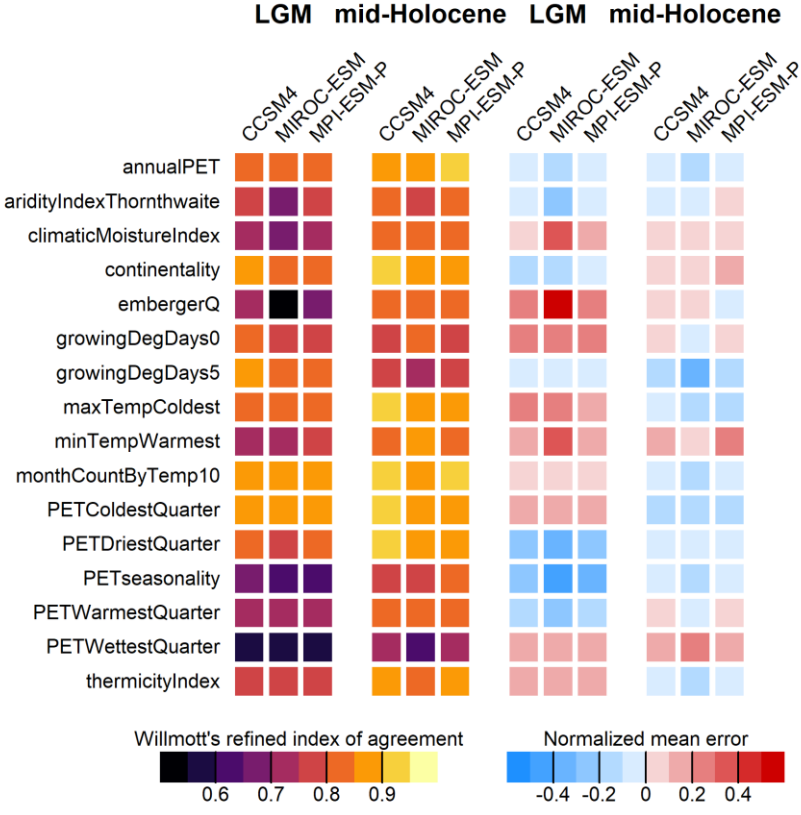

Figure 5: Heat maps showing the agreement between ENVIREM variables derived from the downscaled CCSM3 simulations and those in the ENVIREM database, which are based on simulations from three different GCMs (CCSM4, MIROC-ESM and MPI-ESM-P) for the LGM and mid-Holocene periods. Willmott's refined index of agreement (d_r) indicates the overall agreement of corresponding variables. Normalized ME shows the mean difference between variable values and its direction. A negative value means that the ENVIREM variable presented here has, on average, lower values than the same variable in the ENVIREM database, and vice versa. Both indices were calculated from 10,000 points randomly distributed across Europe.

For the 137 sites across Europe from the Temperature 12k database, both CCSM3 simulations of mean annual temperature and the temperature of the coldest month (January) showed nearly constant warming throughout the Holocene, while pollen-derived temperatures peaked in the mid-Holocene with subsequent cooling (Fig. 6). In contrast, CCSM3 simulations of warmest-month temperatures (July) showed steady Holocene cooling, which agrees with pollen-based reconstructions in the mid and late Holocene, though divergent trends appeared in the early Holocene. However, this discrepancy may be due to the

https://doi.org/10.5194/essd-2026-502
Preprint. Discussion started: 25 November 2026
© Author(s) 2026. CC BY 4.0 License.

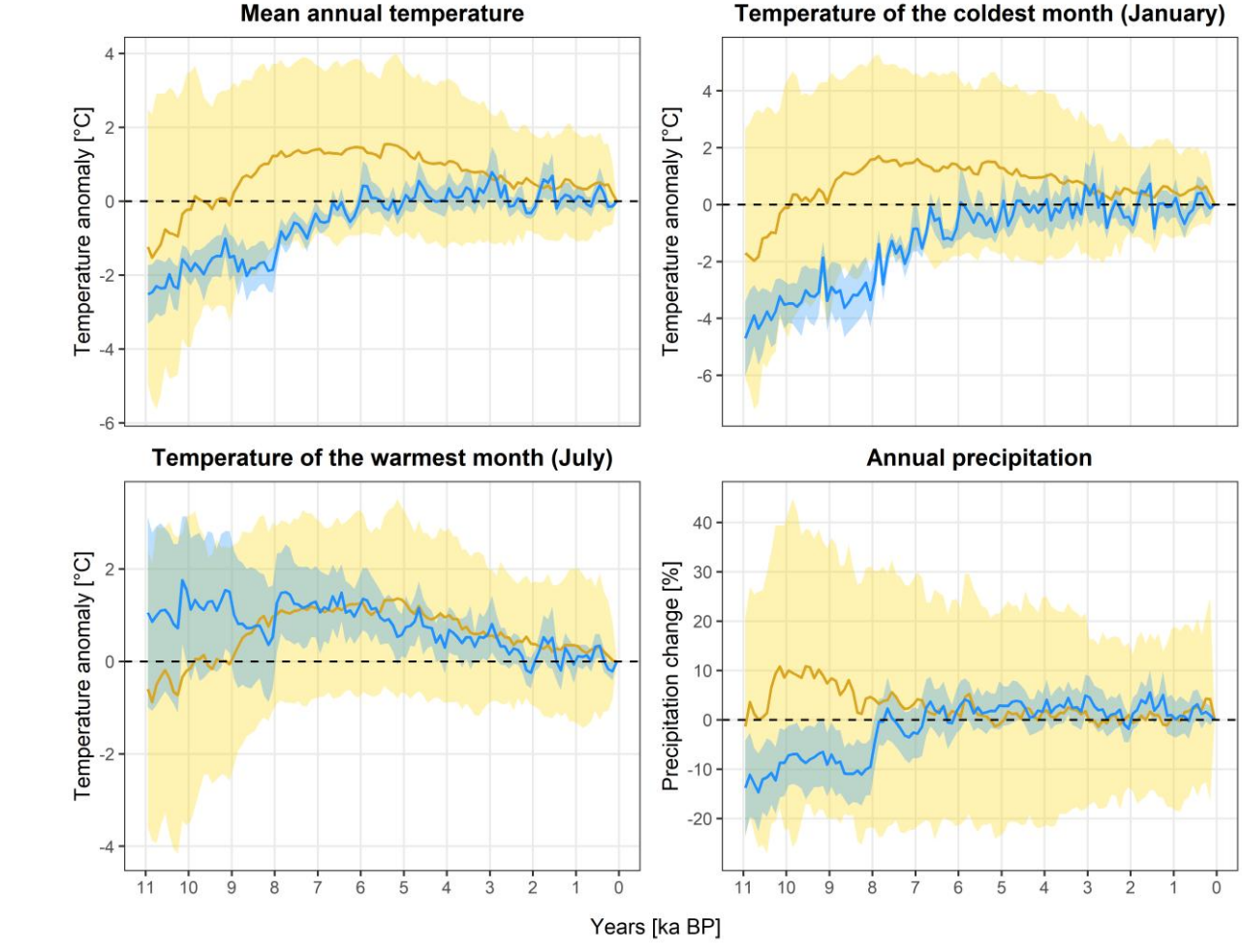

Figure 6: Holocene temperature anomalies and precipitation changes in Europe shown by the downscaled CCSM3 simulations (blue) and pollen-based reconstructions from the Temperature 12k database (yellow). Temperature anomalies and precipitation changes are relative to 100–0 BP (1850–1950 CE). The thick curve represents the mean with 1σ indicated by shading on each side.

When comparing time series of reconstructed and simulated temperature and precipitation values at sites selected from the Temperature 12k database, we found that the agreement between pollen-based reconstructions and CCSM3 simulations is highly region-specific (Fig. 7). For mean annual temperature and the temperature of the coldest month (January), the correlation was highest in central Europe, southern Scandinavia, the British Isles, and the Mediterranean. In contrast, there was high disagreement in the western Alps, northern Scandinavia, and parts of eastern and southeastern Europe. Correlations for the temperature of the warmest month (July) showed a contrasting pattern. The highest agreement between reconstructed

https://doi.org/10.5194/essd-2026-502
Preprint. Discussion started: 25 November 2026
© Author(s) 2026. CC BY 4.0 License.

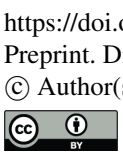

300 and simulated temperatures was found in western temperate Europe and Scandinavia (especially Norway), while the lowest agreement was observed from central Europe to the Balkan Peninsula and eastern Europe but only at a limited number of sites. Temporal trends in annual precipitation rarely matched across the selected sites, especially in the northern Alps, central Europe, and eastern Europe. Only a few sites, particularly in northern and southern Europe, showed a positive correlation between reconstructed and simulated precipitation.

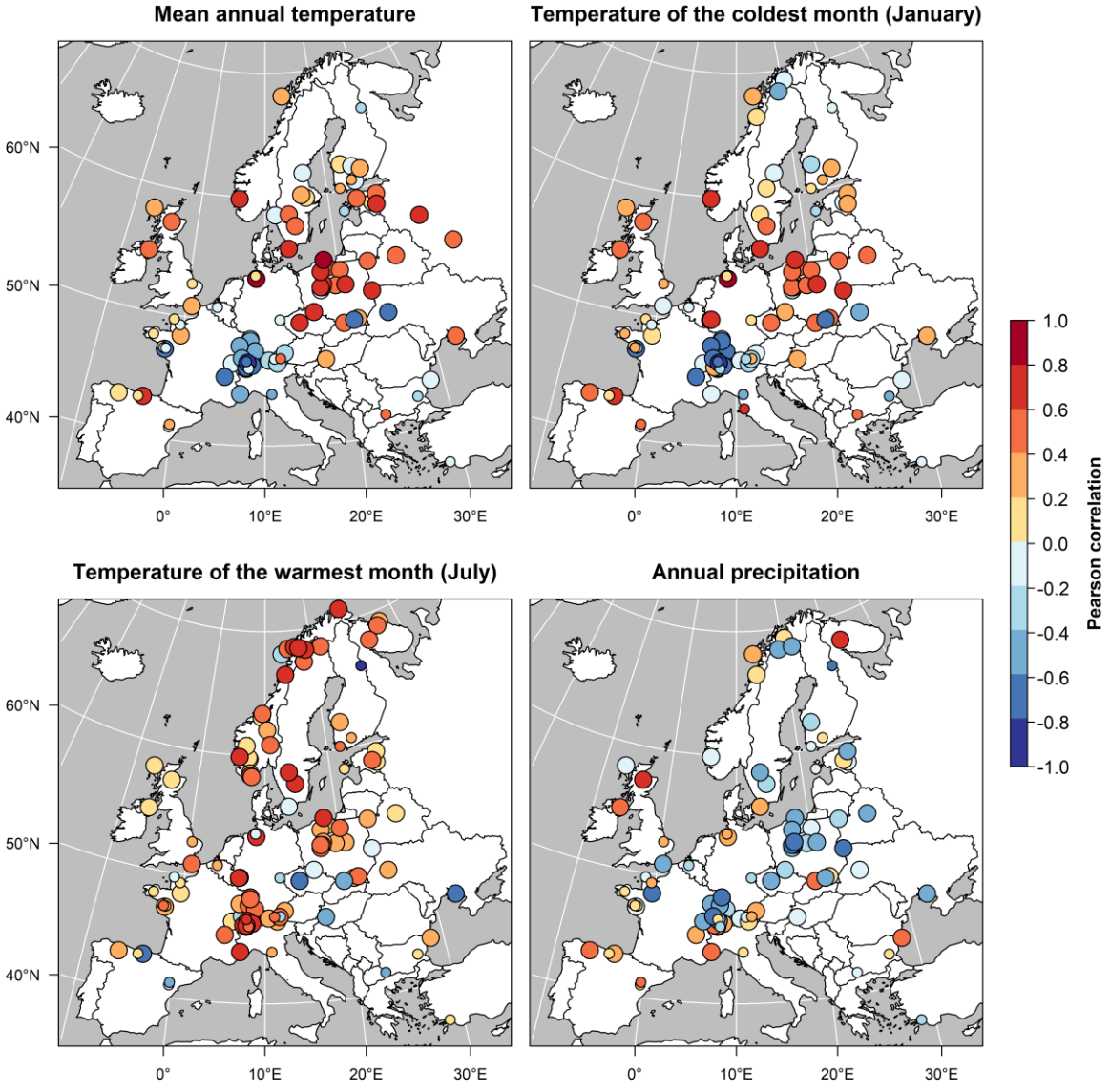

305

Figure 7: Pearson correlations between time series of simulated and reconstructed temperature and precipitation values at each site. Simulated values are from the downscaled CCSM3, while reconstructed values are based on fossil pollen spectra from the Temperature 12k database. The strength and direction of the relationship are indicated by the red–blue color scale. The size of the colored points indicates the length of the time series: larger points represent longer series. Sites with shorter time series are plotted 310 **on top. The maps were created by the authors using state borders from the rworldmap R package (South, 2011).**

https://doi.org/10.5194/essd-2026-502
Preprint. Discussion started: 25 November 2026
© Author(s) 2026. CC BY 4.0 License.

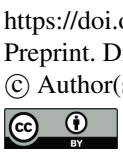

By plotting the strength of correlation between the spatial patterns in reconstructed and simulated temperature and precipitation values within each centennial window, we found a decreasing trend in correlation values from the recent period to the beginning of the Holocene (Fig. 8). In recent periods, the reconstructed and simulated temperature values for selected sites across Europe correlated above 0.75, while in the early Holocene, the correlation values were highly variable, ranging from ~0.1 for mean annual temperature to ~0.5 for the temperature of the coldest month. For annual precipitation, correlation values were generally lower, ranging between ~0.7 in recent periods to ~0.1 in early Holocene.

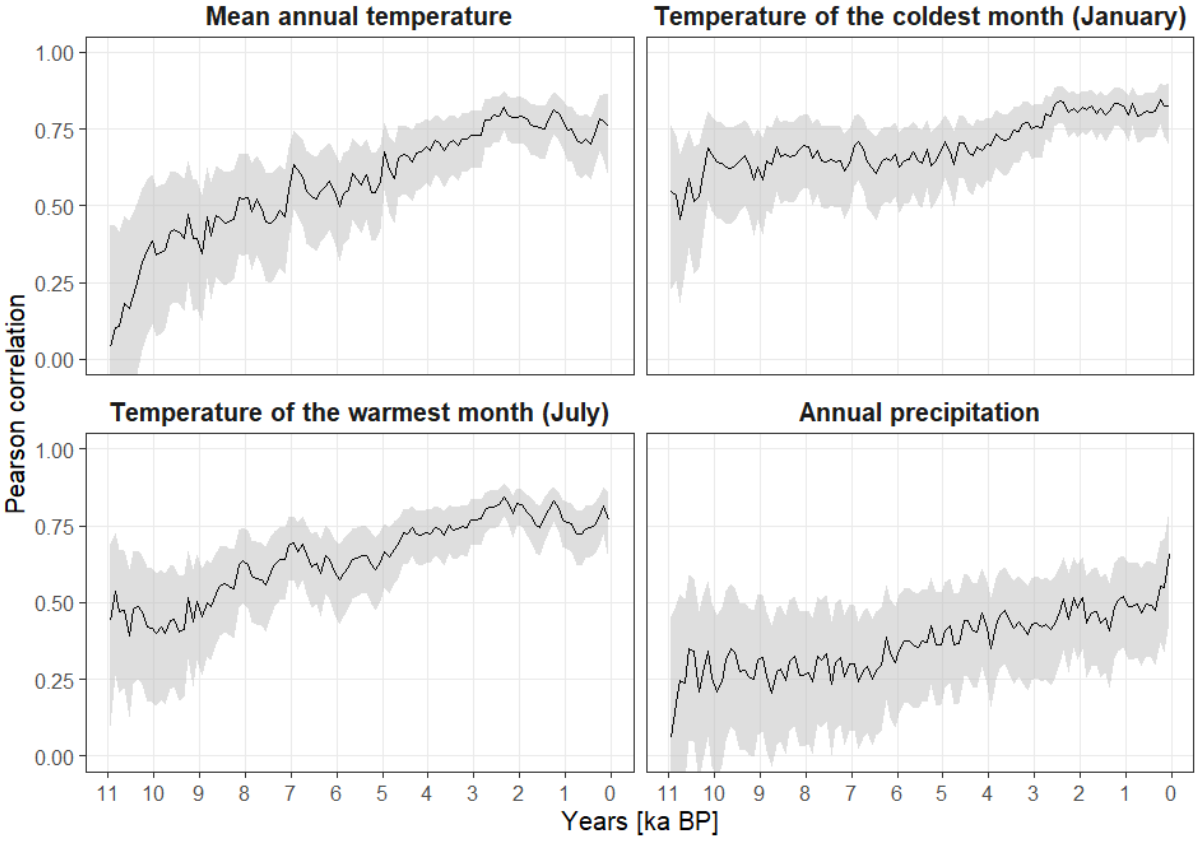

Figure 8: Temporal changes in the strength of the relationship between spatial patterns in simulated and reconstructed temperature and precipitation values across Europe. Simulated values come from the CCSM3 while reconstructed values are based on fossil pollen spectra from the Temperature 12k database. The black line represents the mean correlation value across all sites within each centennial time-window and shading on each side represents 95% confidence interval.

4 Discussion

Paleoclimate simulations from GCMs are widely used across many fields of biological and paleoecological research. A wide range of GCMs is currently available, but CCSM3 has several notable advantages. First, simulations are readily accessible at high temporal resolution directly from TraCE-21k or through the PaleoView software (Fordham et al., 2017), and downscaled

https://doi.org/10.5194/essd-2026-502
Preprint. Discussion started: 25 November 2026
© Author(s) 2026. CC BY 4.0 License.


simulations suitable for paleoecological research at finer landscape scales are also available (Karger et al., 2023). CCSM3 also generally performs well when compared with other GCMs. Previous evaluations show that CCSM3 captures the primary large-scale climatic shifts of the last deglaciation (Liu et al., 2009) while achieving high predictive skill against modern observational records from global meteorological station networks (Fordham et al., 2017). Our work builds on these strengths by downscaling and debiasing CCSM3 simulations and using them to provide high-resolution BIOCLIM and ENVIREM variables suitable for biogeographical and palaeoecological research across European landscapes.

BIOCLIM variables represent a commonly used set of biologically relevant climate data. For the period since the LGM, these variables are available in CHELSA-TraCE21k-centennial-bioclim (Karger et al., 2023) and PaleoClim (Brown et al., 2018) database, both representing simulations of the CCSM3. When validating our BIOCLIM variables against those from these two sources, we found highly congruent spatial patterns and low differences in values of corresponding variables, suggesting that climate evolution and spatial paleoclimate patterns have been successfully captured. Generally, the highest disagreement was found for variables related to the wettest quarter or month (bio8, bio13, bio16, or PETWettestQuarter). This lower agreement likely stems from the inherent sensitivity of these indices to the temporal identification of 'wettest' intervals across different datasets. Bioclimatic variables that combine temperature and precipitation (e.g., bio8) or focus on extreme months are known to produce spatial artifacts and sharp discontinuities, particularly in regions where seasonal precipitation is bimodal or lacks a strong seasonal signal (Booth, 2022; Escobar et al., 2014). Even minor discrepancies in the simulated timing of peak precipitation between models can shift the defined 'wettest' window to different months or quarters. While the underlying monthly values may be comparable, these shifts result in substantial differences in the final indices, thereby reducing the statistical agreement between independent paleoclimatic sources.

ENVIREM variables, originally compiled by Title and Bemmels (2018) based on literature sources, represent another set of variables related to ecological and physiological processes that may directly control species distributions. These include, for example, annual potential evapotranspiration, which is physiologically linked to plant growth potential (Thornthwaite, 1948; Zomer et al., 2006, 2008); the Thornthwaite aridity index, an index of the degree of water deficit (Thornthwaite, 1948); the climatic moisture index, a metric of relative wetness and aridity (Vörösmarty et al., 2005; Willmott and Feddema, 1992); or growing degree-days, which quantify heat sum over the growing season (Metzger et al., 2013). The inclusion of these variables in ecological models often leads to improved model performance and better capture of species' physiological limits compared to standard temperature and precipitation metrics alone (Title and Bemmels, 2018). Indices related to aridity and evapotranspiration are particularly critical for modeling species whose ranges are constrained by water balance, drought and heat stress rather than simple annual means (Crimmins et al., 2011; Stephenson, 1990; Zomer et al., 2008). However, the limited availability of these variables for past periods has hampered their wider use in paleoecology. Here, we bridge this gap by providing these variables as transient time series that directly complement BIOCLIM data, not only from our dataset but also from the aforementioned sources.

The comparison of our downscaled CCSM3 simulations with the Temperature 12k database (Kaufman et al., 2020a) shows that the agreement between model simulations and pollen-based reconstructions varies greatly across both time and space. The

https://doi.org/10.5194/essd-2026-502
Preprint. Discussion started: 25 November 2026
© Author(s) 2026. CC BY 4.0 License.


divergence is most pronounced in the "Holocene temperature conundrum" (Liu et al., 2014b). While pollen-based reconstructions and other proxies indicate that global temperatures likely peaked during a "Thermal Maximum" about 6,500 years ago, followed by a cooling trend in subsequent millennia (Kaufman et al., 2020b; Kaufman and Broadman, 2023), model simulations show lower temperatures during the early Holocene with subsequent steady warming due to rising greenhouse gas concentrations and ice sheet melt. It has been suggested that this divergence may result from the higher sensitivity of biotic proxies to seasonal temperatures rather than to the annual mean (Bova et al., 2021; Liu et al., 2014b). Proxies such as pollen, chironomids, or mollusks reflect climatic factors that directly limit species growth and persistence through physiological processes, such as temperature during the growing season. This is supported, for example, by Marsicek et al. (2018), who showed that the CCSM3 simulation of growing degree days – a measure of accumulated warmth above five degrees – is consistent with inferences from pollen data. In contrast, proxy-inferred winter temperatures may be highly uncertain, thus underestimating the seasonal cycle of temperature (Liu et al., 2025). Our results, although not intended to resolve the Holocene temperature conundrum, support this by showing that the Holocene development of simulated July temperature agrees with pollen-based reconstructions better than simulations of mean annual or January temperature, at least since ~8,000 BP. In addition to temperatures, our results also show surprisingly high agreement between simulated and pollen-inferred mean annual precipitation from about 7,000 BP to the present. This indicates the ability of CCSM3 to capture large-scale temporal fluctuations of annual precipitation across sites with pollen records, although local differences may be significant (see below). The discrepancy between simulated and pollen-inferred temperature and precipitation is not uniform across Europe but highly regionally specific. Spatial correlation patterns show high agreement for mean annual and January temperatures across most of Europe, except for the Alps and some areas in eastern and northern Europe. This suggests that both the CCSM3 simulation and pollen reconstruction accurately capture the broad-scale north–south and Atlantic–continental gradients. However, significant disagreements in the Alps and northern Scandinavia may reflect limitations of the model in capturing complex topographic effects or lingering regional cooling from retreating ice sheets. Additionally, pollen reconstructions in high mountains (and elsewhere) may be confounded by long-distance pollen dispersal, as wind can carry pollen of thermophilous species from lowlands to high elevations and vice versa (Cañellas-Boltà et al., 2009; Markgraf, 1980). In contrast, high agreement for July temperature was found across oceanic regions of Europe but decreased in continental and Mediterranean regions. This discrepancy likely reflects different climatic constraints on vegetation in arid and humid regions, that may confound pollen-based reconstructions (Samartin et al., 2017). While temperature is a primary control for vegetation in humid regions, water availability becomes the limiting factor in more arid regions (Beer et al., 2010; Nemani et al., 2003; Vicente-Serrano et al., 2013). In Mediterranean and continental regions of Europe, the reconstruction of July temperature may thus diverge from CCSM3 simulation due to limited availability of moisture to plants during warm season. Regarding the correlation between precipitation time series, the CCSM3 simulations seem to agree with pollen-based reconstructions in coastal regions of Europe, while inland regions mostly show very low or even negative correlation. This can be attributed to varying local moisture conditions and other factors related to water availability to plants in topographically complex landscapes.

https://doi.org/10.5194/essd-2026-502
Preprint. Discussion started: 25 November 2026
© Author(s) 2026. CC BY 4.0 License.


Temporal trends in the correlation between CCSM3 simulations and pollen-based reconstructions across Europe further highlight the challenges of modeling early Holocene climates and underscore the fundamental importance of seasonal variables (January and July temperatures) over simple annual means, which often mask key ecological processes. While the agreement between simulations and reconstructions is robust for the last few millennia ($r > 0.7$), it declines significantly toward the beginning of the Holocene. For mean annual temperature, the correlation even approaches zero around 11,000 BP. Interestingly, January temperatures maintain a higher and more stable correlation (> 0.6) throughout most of the Holocene. This indicates that winter conditions, which define the northern and altitudinal range limits for frost-sensitive species, are captured with greater reliability than the annual average or summer temperature. Annual precipitation patterns across Europe also show a gradually increasing correlation toward the present, but the mean correlation between CCSM3 simulation and pollen-inferred precipitation did not exceed 0.7. This suggests that although CCSM3 simulation and pollen-inferred precipitation may capture similar broad-scale temporal trends, regional differences may be substantial, resulting in weak correlation.

The provided dataset of 35 paleoclimate variables in centennial steps may be particularly useful for many fields of ecological research, including Species (Paleo)Distribution Modeling (SDM), demographic simulations or the development of new calibration systems for reconstructing past climates from proxy data. While traditional SDMs often transfer present-day correlations to the past under the assumption of niche conservatism, evidence of niche shifts (e.g. Veloz et al., 2012) can undermine this approach. By offering high-resolution data across consecutive windows, our dataset enables 'multi-temporal model calibration' (Nogués-Bravo, 2009), which captures the full spectrum of climatic conditions a species has occupied over time. This approach, especially when combined with variables that have direct mechanistic links to survival and reproduction, may significantly enhance model transferability across different periods by reflecting fundamental environmental constraints of species niche (Yates et al., 2018). Furthermore, these data facilitate spatially explicit demographic and migration simulations in which migration barriers and habitat suitability are treated as dynamic variables (Bemmels et al., 2019; Divíšek et al., 2022). The practical utility of transient climate simulations may be demonstrated by tracking past climatically triggered colonization and extinction events. For example, Horsák et al. (2020) showed that a short period of abrupt cooling and drying around 8,500 BP delayed the colonization of Western Europe by forest land snails from glacial refugia located in Eastern Europe (Juřičková et al., 2014a). Moreover, climatic aridity in Western Europe was identified as the main driver of local species-richness patterns during the Holocene, while in Central Europe, minimum January temperature was the primary driver. Similarly, the ability of simulated summer precipitation to explain colonization and extinction events for two species of the genus *Pyramidula* in the Western Carpathians was demonstrated by Horsáková et al. (2024).

5 Data availability

The dataset of gridded high-resolution BIOCLIM and ENVIREM variables in GeoTIFF format is available at https://doi.org/10.5281/zenodo.5119958 (Divíšek, 2021). All raster layers use a geographic coordinate system referenced to

https://doi.org/10.5194/essd-2026-502
Preprint. Discussion started: 25 November 2026
© Author(s) 2026. CC BY 4.0 License.



the WGS 84 horizontal datum [EPSG 4326: +proj=longlat +datum=WGS84 +no_defs] and have a resolution of 0.0083333333°. File naming conventions are described in Technical specification: https://zenodo.org/records/5119958/files/Technical_specification.pdf?download=1.

6 Code availability

R scripts used in the downscaling procedure and for calculating BIOCLIM and ENVIREM variables are available at https://doi.org/10.5281/zenodo.24500021 (Divíšek, 2026). Scripts used to compare the downscaled CCSM3 simulations with proxy-inferred reconstructions and other GCM simulations are available for review at https://github.com/jdivisek/CCSM3vsPollen and will be permanently and publicly archived in the Zenodo repository upon acceptance of the paper.

7 Conclusions

This study presents a dataset of 35 biologically relevant climate variables documenting the climatic evolution of Europe over the last 21,000 years in centennial increments. This dataset bridges the gap between coarse-grained global circulation models and the high-resolution requirements of modern biogeographical and paleoecological research. Our comparison of the downscaled CCSM3 simulations with the Temperature 12k database reveals that agreement between model outputs and pollen records is highly variable across both time and space. We also show that these (dis)agreements depend on whether annual means or seasonal variables are considered. The resulting dataset, provided as an open-access resource, offers a solid foundation for future studies focused on a deeper understanding of the climate-driven mechanisms that have shaped contemporary European biodiversity.

Author contributions

All authors conceptualized the study. JD performed the analyses, validation, visualized the results, and wrote the manuscript. All authors interpreted the results. MHá, MHo, and PH contributed to the writing. PH acquired funding.

Competing interests

The authors declare that they have no conflict of interest.

https://doi.org/10.5194/essd-2026-502
Preprint. Discussion started: 25 November 2026
© Author(s) 2026. CC BY 4.0 License.



Open Access Earth System Science Data Discussions

Disclaimer

Copernicus Publications remains neutral with regard to jurisdictional claims made in the text, published maps, institutional affiliations, or any other geographical representation in this paper. While Copernicus Publications makes every effort to include appropriate place names, the final responsibility lies with the authors. Views expressed in the text are those of the authors and do not necessarily reflect the views of the publisher.

Financial support

This work was supported by the Czech Science Foundation project no. GA23-05132S. PH was additionally supported by the Czech Academy of Sciences (the long-term developmental project RVO 67985939).

References

Alley, R. B. and Ágústsdóttir, A. M.: The 8k event: cause and consequences of a major Holocene abrupt climate change, Quaternary Sci Rev, 24, 1123–1149, https://doi.org/10.1016/j.quascirev.2004.12.004, 2005.

Beer, C., Reichstein, M., Tomelleri, E., Ciais, P., Jung, M., Carvalhais, N., Rödenbeck, C., Arain, M. A., Baldocchi, D., Bonan, G. B., Bondeau, A., Cescatti, A., Lasslop, G., Lindroth, A., Lomas, M., Luyssaert, S., Margolis, H., Oleson, K. W., Roupsard, O., Veenendaal, E., Viovy, N., Williams, C., Woodward, F. I., and Papale, D.: Terrestrial gross carbon dioxide uptake: global distribution and covariation with climate, Science, 329, 834–838, https://doi.org/10.1126/science.1184984, 2010.

Bemmels, J. B., Knowles, L. L., and Dick, C. W.: Genomic evidence of survival near ice sheet margins for some, but not all, North American trees, PNAS, 116, 8431–8436, https://doi.org/10.1073/pnas.1901656116, 2019.

Bennett, K. D., Tzedakis, P. C., and Willis, K. J.: Quaternary refugia of north European trees, J Biogeogr, 18, 103–115, https://doi.org/10.2307/2845248, 1991.

Blois, J. L., Williams, J. W., Fitzpatrick, M. C., Ferrier, S., Veloz, S. D., He, F., Liu, Z., Manion, G., and Otto-Bliesner, B.: Modeling the climatic drivers of spatial patterns in vegetation composition since the Last Glacial Maximum, Ecography, 36, 460–473, https://doi.org/10.1111/j.1600-0587.2012.07852.x, 2013a.

Blois, J. L., Williams, J. W., Fitzpatrick, M. C., Jackson, S. T., and Ferrier, S.: Space can substitute for time in predicting climate-change effects on biodiversity, PNAS, 110, 9374–9379, https://doi.org/10.1073/pnas.1220228110, 2013b.

Boomgard-Zagrodnik, J. P. and Brown, D. J.: Machine learning imputation of missing Mesonet temperature observations, Comput Electron Agr, 192, 106580, https://doi.org/10.1016/j.compag.2021.106580, 2022.

Booth, T. H.: Checking bioclimatic variables that combine temperature and precipitation data before their use in species distribution models, Austral Ecol, 47, 1506–1514, https://doi.org/10.1111/aec.13234, 2022.

Bova, S., Rosenthal, Y., Liu, Z., Godad, S. P., and Yan, M.: Seasonal origin of the thermal maxima at the Holocene and the last interglacial, Nature, 589, 548–553, https://doi.org/10.1038/s41586-020-03155-x, 2021.

https://doi.org/10.5194/essd-2026-502
Preprint. Discussion started: 25 November 2026
© Author(s) 2026. CC BY 4.0 License.



Brenning, A., Bangs, D., and Becker, M.: RSAGA: SAGA geoprocessing and terrain analysis, CRAN [code] https://CRAN.R-project.org/package=RSAGA, 2018.

Brown, J. L., Hill, D. J., Dolan, A. M., Carnaval, A. C., and Haywood, A. M.: PaleoClim, high spatial resolution paleoclimate surfaces for global land areas, Sci Data, 5, 180254, https://doi.org/10.1038/sdata.2018.254, 2018.

Cañellas-Boltà, N., Rull, V., Vigo, J., and Mercadé, A.: Modern pollen—vegetation relationships along an altitudinal transect in the central Pyrenees (southwestern Europe), Holocene, 19, 1185–1200, https://doi.org/10.1177/0959683609345082, 2009.

Cannon, A. J., Sobie, S. R., and Murdock, T. Q.: Bias correction of GCM precipitation by quantile mapping: how well do methods preserve changes in quantiles and extremes?, J Climate, 28, 6938–6959, https://doi.org/10.1175/JCLI-D-14-00754.1, 2015.

Collins, W. D., Bitz, C. M., Blackmon, M. L., Bonan, G. B., Bretherton, C. S., Carton, J. A., Chang, P., Doney, S. C., Hack, J. J., Henderson, T. B., Kiehl, J. T., Large, W. G., McKenna, D. S., Santer, B. D., and Smith, R. D.: The Community Climate System Model version 3 (CCSM3), J Climate, 19, 2122–2143, https://doi.org/10.1175/JCLI3761.1, 2006.

Conrad, O., Bechtel, B., Bock, M., Dietrich, H., Fischer, E., Gerlitz, L., Wehberg, J., Wichmann, V., and Böhner, J.: System for automated geoscientific analyses (SAGA) v. 2.1.4, Geosci Model Dev, 8, 2271–2312, https://doi.org/10.5194/gmdd-8-2271-2015, 2015.

Cooper, A., Turney, C., Hughen, K. A., Brook, B. W., McDonald, H. G., and Bradshaw, C. J. A.: Abrupt warming events drove Late Pleistocene Holarctic megafaunal turnover, Science, 349, 602–606, https://doi.org/10.1126/science.aac4315, 2015.

Crimmins, S. M., Dobrowski, S. Z., Greenberg, J. A., Abatzoglou, J. T., and Mynsberge, A. R.: Changes in climatic water balance drive downhill shifts in plant species' optimum elevations, Science, 331, 324–327, https://doi.org/10.1126/science.1199040, 2011.

Crucifix, M.: palinsol: insolation for palaeoclimate studies, CRAN [code], https://CRAN.R-project.org/package=palinsol, 2016.

Divíšek, J.: High-resolution BIOCLIM and ENVIREM grids for Europe in consecutive 100-year bins spanning the last 21,000 years, Zenodo [data set], https://doi.org/10.5281/zenodo.5119958, 2021.

Divíšek, J.: R scripts for statistical downscaling of CCSM3 (TraCE-21ka) paleoclimate simulations over Europe (Version v1.0.0), Zenodo [code], https://doi.org/10.5281/zenodo.24500021, 2026.

Divíšek, J., Večeřa, M., Welk, E., Danihelka, J., Chytrý, K., Douda, J., and Chytrý, M.: Origin of the central European steppe flora: insights from palaeodistribution modelling and migration simulations, Ecography, 2022, e06293, https://doi.org/10.1111/ecog.06293, 2022.

Escobar, L. E., Lira-Noriega, A., Medina-Vogel, G., and Townsend Peterson, A.: Potential for spread of the white-nose fungus (Pseudogymnoascus destructans) in the Americas: use of Maxent and NicheA to assure strict model transference, Geospat Health, 9, 221, https://doi.org/10.4081/gh.2014.19, 2014.

https://doi.org/10.5194/essd-2026-502
Preprint. Discussion started: 25 November 2026
© Author(s) 2026. CC BY 4.0 License.

Fordham, D. A., Saltré, F., Haythorne, S., Wigley, T. M. L., Otto-Bliesner, B. L., Chan, K. C., and Brook, B. W.: PaleoView: a tool for generating continuous climate projections spanning the last 21 000 years at regional and global scales, Ecography, 40, 1348–1358, https://doi.org/10.1111/ecog.03031, 2017.

Fordham, D. A., Saltré, F., Brown, S. C., Mellin, C., and Wigley, T. M. L.: Why decadal to century timescale palaeoclimate data are needed to explain present-day patterns of biological diversity and change, Glob Change Biol, 24, 1371–1381, https://doi.org/10.1111/gcb.13932, 2018.

Fordham, D. A., Jackson, S. T., Brown, S. C., Huntley, B., Brook, B. W., Dahl-Jensen, D., Gilbert, M. T. P., Otto-Bliesner, B. L., Svensson, A., Theodoridis, S., Wilmshurst, J. M., Buettel, J. C., Canteri, E., McDowell, M., Orlando, L., Pilowsky, J. A., Rahbek, C., and Nogues-Bravo, D.: Using paleo-archives to safeguard biodiversity under climate change, Science, 369, eabc5654, https://doi.org/10.1126/science.abc5654, 2020.

Hewitt, G.: The genetic legacy of the Quaternary ice ages, Nature, 405, 907–913, https://doi.org/10.1038/35016000, 2000.

Hijmans, R. J.: raster: geographic data analysis and modeling, CRAN [code], https://CRAN.R-project.org/package=raster, 2019.

Hijmans, R. J., Cameron, S. E., Parra, J. L., Jones, P. G., and Jarvis, A.: Very high resolution interpolated climate surfaces for global land areas, Int. J. Climatol., 25, 1965–1978, https://doi.org/10.1002/joc.1276, 2005.

Horsák, M., Limondin-Lozouet, N., Granai, S., Dabkowski, J., Divíšek, J., and Hájková, P.: Colonisation dynamic and diversity patterns of Holocene forest snail fauna across temperate Europe: the imprint of palaeoclimate changes, Quaternary Sci Rev, 240, 106367, https://doi.org/10.1016/j.quascirev.2020.106367, 2020.

Horsáková, V., Divíšek, J., Líznarová, E., Kubíková, K., Juřičková, L., and Horsák, M.: Alpine travellers in the Carpathians: the story of two rock-dwelling snails told by genes and fossils, J Biogeogr, 51, 1693–1708, https://doi.org/10.1111/jbi.14793, 2024.

Juřičková, L., Horáčková, J., and Ložek, V.: Direct evidence of central European forest refugia during the last glacial period based on mollusc fossils, Quaternary Res, 82, 222–228, https://doi.org/10.1016/j.yqres.2014.01.015, 2014a.

Juřičková, L., Horsák, M., Horáčková, J., Abraham, V., and Ložek, V.: Patterns of land-snail succession in Central Europe over the last 15,000 years: main changes along environmental, spatial and temporal gradients, Quaternary Sci Rev, 93, 155–166, https://doi.org/10.1016/j.quascirev.2014.03.019, 2014b.

Karger, D. N., Conrad, O., Böhner, J., Kawohl, T., Kreft, H., Soria-Auza, R. W., Zimmermann, N. E., Linder, H. P., and Kessler, M.: Climatologies at high resolution for the earth's land surface areas, Sci Data, 4, 170122, https://doi.org/10.1038/sdata.2017.122, 2017.

Karger, D. N., Nobis, M. P., Normand, S., Graham, C. H., and Zimmermann, N. E.: CHELSA-TraCE21k – high-resolution (1 km) downscaled transient temperature and precipitation data since the Last Glacial Maximum, Clim Past, 19, 439–456, https://doi.org/10.5194/cp-19-439-2023, 2023.

Kaufman, D., McKay, N., Routson, C., Erb, M., Davis, B., Heiri, O., Jaccard, S., Tierney, J., Dätwyler, C., Axford, Y., Brussel, T., Cartapanis, O., Chase, B., Dawson, A., Vernal, A. de, Engels, S., Jonkers, L., Marsicek, J., Moffa-Sánchez, P., Morrill, C.,

https://doi.org/10.5194/essd-2026-502
Preprint. Discussion started: 25 November 2026
© Author(s) 2026. CC BY 4.0 License.

Orsi, A., Rehfeld, K., Saunders, K., Sommer, P. S., Thomas, E., Tonello, M., Tóth, M., Vachula, R., Andreev, A., Bertrand, S., Biskaborn, B., Bringué, M., Brooks, S., Caniupán, M., Chevalier, M., Cwynar, L., Emile-Geay, J., Fegyveresi, J., Feurdean, A., Finsinger, W., Fortin, M.-C., Foster, L., Fox, M., Gajewski, K., Grosjean, M., Hausmann, S., Heinrichs, M., Holmes, N., Ilyashuk, B., Ilyashuk, E., Juggins, S., Khider, D., Koinig, K., Langdon, P., Larocque-Tobler, I., Li, J., Lotter, A., Luoto, T., Mackay, A., Magyari, E., Malevich, S., Mark, B., Massaferro, J., Montade, V., Nazarova, L., Novenko, E., Pařil, P., Pearson, E., Peros, M., Pienitz, R., Płóciennik, M., Porinchu, D., Potito, A., Rees, A., Reinemann, S., Roberts, S., Rolland, N., Salonen, S., Self, A., Seppä, H., Shala, S., St-Jacques, J.-M., Stenni, B., Syrykh, L., Tarrats, P., Taylor, K., Bos, V. van den, Velle, G., Wahl, E., Walker, I., Wilmshurst, J., Zhang, E., and Zhilich, S.: A global database of Holocene paleotemperature records, Sci Data, 7, 1–34, https://doi.org/10.1038/s41597-020-0445-3, 2020a.

Kaufman, D., McKay, N., Routson, C., Erb, M., Dätwyler, C., Sommer, P. S., Heiri, O., and Davis, B.: Holocene global mean surface temperature, a multi-method reconstruction approach, Sci Data, 7, 201, https://doi.org/10.1038/s41597-020-0530-7, 2020b.

Kaufman, D. S. and Broadman, E.: Revisiting the Holocene global temperature conundrum, Nature, 614, 425–435, https://doi.org/10.1038/s41586-022-05536-w, 2023.

Lalic, B., Stapleton, A., Vergauwen, T., Caluwaerts, S., Eichelmann, E., and Roantree, M.: A comparative analysis of machine learning approaches to gap filling meteorological datasets, Environ Earth Sci, 83, 679, https://doi.org/10.1007/s12665-024-11982-8, 2024.

Lambeck, K., Rouby, H., Purcell, A., Sun, Y., and Sambridge, M.: Sea level and global ice volumes from the Last Glacial Maximum to the Holocene, PNAS, 111, 15296–15303, https://doi.org/10.1073/pnas.1411762111, 2014.

Lee, S., Wolberg, G., and Shin, S. Y.: Scattered data interpolation with multilevel B-splines, IEEE T Vis Comput Gr, 3, 228–244, https://doi.org/10.1109/2945.620490, 1997.

Liu, Z., Otto-Bliesner, B. L., He, F., Brady, E. C., Tomas, R., Clark, P. U., Carlson, A. E., Lynch-Stieglitz, J., Curry, W., Brook, E., Erickson, D., Jacob, R., Kutzbach, J., and Cheng, J.: Transient simulation of last deglaciation with a new mechanism for Bølling-Allerød warming, Science, 325, 310–314, https://doi.org/10.1126/science.1171041, 2009.

Liu, Z., Lu, Z., Wen, X., Otto-Bliesner, B. L., Timmermann, A., and Cobb, K. M.: Evolution and forcing mechanisms of El Niño over the past 21,000 years, Nature, 515, 550–553, https://doi.org/10.1038/nature13963, 2014a.

Liu, Z., Zhu, J., Rosenthal, Y., Zhang, X., Otto-Bliesner, B. L., Timmermann, A., Smith, R. S., Lohmann, G., Zheng, W., and Timm, O. E.: The Holocene temperature conundrum, PNAS, 111, E3501–E3505, https://doi.org/10.1073/pnas.1407229111, 2014b.

Liu, Z., Cheng, J., Zheng, Y., Zhang, W., Liu, H., Wu, H., Zhu, J., and Xie, S.: The seasonal temperature conundrum for the Holocene, Sci Adv, 11, eadt8950, https://doi.org/10.1126/sciadv.adt8950, 2025.

Lorenz, D. J., Nieto-Lugilde, D., Blois, J. L., Fitzpatrick, M. C., and Williams, J. W.: Downscaled and debiased climate simulations for North America from 21,000 years ago to 2100AD, Sci Data, 3, 1–19, https://doi.org/10.1038/sdata.2016.48, 2016.

https://doi.org/10.5194/essd-2026-502
Preprint. Discussion started: 25 November 2026
© Author(s) 2026. CC BY 4.0 License.

Ložek, V.: Quartärmollusken der Tschechoslowakei, Rozpravy Ústředního ústavu geologického, 31, 1964.

Magny, M., Vannière, B., Zanchetta, G., Fouache, E., Touchais, G., Petrika, L., Coussot, C., Walter-Simonnet, A.-V., and Arnaud, F.: Possible complexity of the climatic event around 4300—3800 cal. BP in the central and western Mediterranean, Holocene, 19, 823–833, https://doi.org/10.1177/0959683609337360, 2009.

Maraun, D.: Bias correction, quantile mapping, and downscaling: revisiting the inflation issue, J Climate, 26, 2137–2143, https://doi.org/10.1175/JCLI-D-12-00821.1, 2013.

Markgraf, V.: Pollen dispersal in a mountain area, Grana, 19, 127–146, https://doi.org/10.1080/00173138009424995, 1980.

Marsicek, J., Shuman, B. N., Bartlein, P. J., Shafer, S. L., and Brewer, S.: Reconciling divergent trends and millennial variations in Holocene temperatures, Nature, 554, 92–96, https://doi.org/10.1038/nature25464, 2018.

Mayewski, P. A., Rohling, E. E., Curt Stager, J., Karlén, W., Maasch, K. A., David Meeker, L., Meyerson, E. A., Gasse, F., van Kreveld, S., Holmgren, K., Lee-Thorp, J., Rosqvist, G., Rack, F., Staubwasser, M., Schneider, R. R., and Steig, E. J.: Holocene climate variability, Quaternary Res, 62, 243–255, https://doi.org/10.1016/j.yqres.2004.07.001, 2004.

Metzger, M. J., Bunce, R. G. H., Jongman, R. H. G., Sayre, R., Trabucco, A., and Zomer, R.: A high-resolution bioclimate map of the world: a unifying framework for global biodiversity research and monitoring, Global Ecol Biogeogr, 22, 630–638, https://doi.org/https://doi.org/10.1111/geb.12022, 2013.

Moreno, A. and Hasenauer, H.: Spatial downscaling of European climate data, Int. J. Climatol., 36, 1444–1458, https://doi.org/10.1002/joc.4436, 2016.

Nemani, R. R., Keeling, C. D., Hashimoto, H., Jolly, W. M., Piper, S. C., Tucker, C. J., Myneni, R. B., and Running, S. W.: Climate-driven increases in global terrestrial net primary production from 1982 to 1999, Science, 300, 1560–1563, https://doi.org/10.1126/science.1082750, 2003.

Nix, H. A.: A biogeographic analysis of Australian elapid snakes, in: Atlas of elapid snakes of Australia, Australian Government Publishing Service, Canberra, 4–15, 1986.

Nogués-Bravo, D.: Predicting the past distribution of species climatic niches, Global Ecol Biogeogr, 18, 521–531, https://doi.org/10.1111/j.1466-8238.2009.00476.x, 2009.

Otto-Bliesner, B. L., Tomas, R., Brady, E. C., Ammann, C., Kothavala, Z., and Clauzet, G.: Climate sensitivity of moderate- and low-resolution versions of CCSM3 to preindustrial forcings, J Climate, 19, 2567–2583, https://doi.org/10.1175/JCLI3754.1, 2006.

Otto-Bliesner, B. L., Russell, J. M., Clark, P. U., Liu, Z., Overpeck, J. T., Konecky, B., deMenocal, P., Nicholson, S. E., He, F., and Lu, Z.: Coherent changes of southeastern equatorial and northern African rainfall during the last deglaciation, Science, 346, 1223–1227, https://doi.org/10.1126/science.1259531, 2014.

R Core Team: R: A language and environment for statistical computing, https://www.r-project.org/, 2022.

Ramirez Villejas, J. and Jarvis, A.: Downscaling global circulation model outputs: the delta method decision and policy analysis working paper No. 1., International Center for Tropical Agriculture (CIAT). Cali. CO., 2010.

https://doi.org/10.5194/essd-2026-502
Preprint. Discussion started: 25 November 2026
© Author(s) 2026. CC BY 4.0 License.



Samartin, S., Heiri, O., Joos, F., Renssen, H., Franke, J., Brönnimann, S., and Tinner, W.: Warm Mediterranean mid-Holocene summers inferred from fossil midge assemblages, Nat Geosci, 10, 207–212, https://doi.org/10.1038/ngeo2891, 2017.

Schmitt, T. and Varga, Z.: Extra-Mediterranean refugia: the rule and not the exception?, Front Zool, 9, 22, https://doi.org/10.1186/1742-9994-9-22, 2012.

South, A.: rworldmap: a new R package for mapping global data, R J, 3, 35–43, https://doi.org/10.32614/RJ-2011-006, 2011.

Stekhoven, D. J. and Bühlmann, P.: MissForest—non-parametric missing value imputation for mixed-type data, Bioinformatics, 28, 112–118, https://doi.org/10.1093/bioinformatics/btr597, 2012.

Stephenson, N. L.: Climatic control of vegetation distribution: the role of the water balance, Am Nat, 135, 649–670, https://doi.org/10.1086/285067, 1990.

Svenning, J. C., Eiserhardt, W. L., Normand, S., Ordonez, A., and Sandel, B.: The influence of paleoclimate on present-day patterns in biodiversity and ecosystems, Annu Rev Ecol Evol Syst, 46, 551–572, https://doi.org/10.1146/ANNUREV-ECOLSYS-112414-054314, 2015.

Thornthwaite, C. W.: An approach toward a rational classification of climate, Geogr Rev, 38, 55–94, https://doi.org/10.2307/210739, 1948.

Title, P. O. and Bemmels, J. B.: ENVIREM: an expanded set of bioclimatic and topographic variables increases flexibility and improves performance of ecological niche modeling, Ecography, 41, 291–307, https://doi.org/10.1111/ecog.02880, 2018.

Veloz, S. D., Williams, J. W., Blois, J. L., He, F., Otto-Bliesner, B., and Liu, Z.: No-analog climates and shifting realized niches during the late quaternary: implications for 21st-century predictions by species distribution models, Glob Change Biol, 18, 1698–1713, https://doi.org/https://doi.org/10.1111/j.1365-2486.2011.02635.x, 2012.

Vicente-Serrano, S. M., Gouveia, C., Camarero, J. J., Beguería, S., Trigo, R., López-Moreno, J. I., Azorín-Molina, C., Pasho, E., Lorenzo-Lacruz, J., Revuelto, J., Morán-Tejeda, E., and Sanchez-Lorenzo, A.: Response of vegetation to drought time-scales across global land biomes, PNAS, 110, 52–57, https://doi.org/10.1073/pnas.1207068110, 2013.

Vörösmarty, C. J., Douglas, E. M., Green, P. A., and Revenga, C.: Geospatial indicators of emerging water stress: an application to Africa, ambi, 34, 230–236, https://doi.org/10.1579/0044-7447-34.3.230, 2005.

Williams, J. W., Shuman, B. N., Webb III, T., Bartlein, P. J., and Leduc, P. L.: Late-Quaternary vegetation dynamics in North America: scaling from taxa to biomes, Ecol Monogr, 74, 309–334, https://doi.org/10.1890/02-4045, 2004.

Willmott, C. J. and Feddema, J. J.: A more rational climatic moisture index, Prof Geogr, 44, 84–88, https://doi.org/https://doi.org/10.1111/j.0033-0124.1992.00084.x, 1992.

Willmott, C. J., Robeson, S. M., and Matsuura, K.: A refined index of model performance, Int J Climatol, 32, 2088–2094, https://doi.org/10.1002/joc.2419, 2012.

Xu, T. and Hutchinson, M. F.: ANUCLIM version 6.1, https://fennerschool.anu.edu.au/research/products/anuclim-version-6-1, 2011.

Yates, K. L., Bouchet, P. J., Caley, M. J., Mengersen, K., Randin, C. F., Parnell, S., Fielding, A. H., Bamford, A. J., Ban, S., Barbosa, A. M., Dormann, C. F., Elith, J., Embling, C. B., Ervin, G. N., Fisher, R., Gould, S., Graf, R. F., Gregr, E. J., Halpin,

https://doi.org/10.5194/essd-2026-502
Preprint. Discussion started: 25 November 2026
© Author(s) 2026. CC BY 4.0 License.



P. N., Heikkinen, R. K., Heinänen, S., Jones, A. R., Krishnakumar, P. K., Lauria, V., Lozano-Montes, H., Mannocci, L., Mellin, C., Mesgaran, M. B., Moreno-Amat, E., Mormede, S., Novaczek, E., Oppel, S., Ortuño Crespo, G., Peterson, A. T., Rapacciuolo, G., Roberts, J. J., Ross, R. E., Scales, K. L., Schoeman, D., Snelgrove, P., Sundblad, G., Thuiller, W., Torres, L. G., Verbruggen, H., Wang, L., Wenger, S., Whittingham, M. J., Zharikov, Y., Zurell, D., and Sequeira, A. M. M.: Outstanding challenges in the transferability of ecological models, Trends Ecol Evol, 33, 790–802, https://doi.org/10.1016/j.tree.2018.08.001, 2018.

Yeager, S. G., Shields, C. A., Large, W. G., and Hack, J. J.: The low-resolution CCSM3, J Climate, 19, 2545–2566, https://doi.org/10.1175/JCLI3744.1, 2006.

Zambrano-Bigiarini, M.: hydroGOF: Goodness-of-fit functions for comparison of simulated and observed hydrological time series. R package version 0.7-0, CRAN [code], https://CRAN.R-project.org/package=hydroGOF, 2026.

Zomer, R., Trabucco, A., van Straaten, O., and Bossio, D.: Carbon, land and water: a global analysis of the hydrologic dimensions of climate change mitigation through afforestation / reforestation, International Water Management Institute, Colombo, Sri Lanka, 44pp, 2006.

Zomer, R. J., Trabucco, A., Bossio, D. A., and Verchot, L. V.: Climate change mitigation: a spatial analysis of global land suitability for clean development mechanism afforestation and reforestation, Agr Ecosyst Environ, 126, 67–80, https://doi.org/10.1016/j.agee.2008.01.014, 2008.